

Source time functions of earthquakes based on a stochastic differential equation

Shiro Hirano

Source time functions are essential observable quantities in seismology; they have been investigated via kinematic inversion analyses and compiled into databases. Given the numerous available results, some empirical laws on source time functions have been established, even though they are complicated and fluctuate along time series. Theoretically, stochastic differential equations, which include a random variable and white noise, are suitable for modeling such complicated phenomena. In this study, we model source time functions as the convolution of two stochastic processes (known as Bessel processes). We mathematically and numerically demonstrate that this convolution satisfies some of the empirical laws of source time functions, including non-negativity, finite duration, unimodality, a growth rate proportional to t^3 , ω^{-2} -type spectra, and frequency distribution. We interpret this convolution and speculate that the stress drop rate and fault impedance follow the same Bessel process.

16 **1 Introduction**

17 Earthquake source time functions (STFs), which are temporal variations in the slip rate integrated over
18 faults during earthquakes, are macroscopically observable in seismology and have been widely investi-
19 gated regarding kinematic source inversions and dynamic source modeling. To review some knowledge
20 on STFs, we first summarize some empirical laws (ELs) for STFs:

21 **EL1** STFs are dominantly non-negative, continuous, compactly supported, and unimodal.

22 **EL2** The moment functions, which are proportional to the time-integration of STFs, evolve as $\sim t^3$,
23 where t is the time since their ignition (this is referred to as “the cube law” herein).

24 **EL3** The ω^{-2} -model can satisfactorily approximate the amplitude of STF Fourier spectra.

25 **EL4** The frequency of their total moment follows the Gutenberg-Richter (GR) law.

26 Many studies, from early pioneering research [e.g., *Houston*, 2001] to recent revelations [e.g., *Yin*
27 *et al.*, 2021] have cataloged numerous STFs and revealed their tendencies and variabilities over time.
28 Although several outliers have been found, EL1 has arisen as an obvious tendency, based on cataloged
29 data. For example, $\sim 80\%$ of the cataloged STFs are unimodal; they are labeled Group 1 in the research
30 of *Yin et al.* [2021]. In EL1, the fact that STFs are compactly supported is natural because regular earth-
31 quakes terminate within a few minutes, whereas slow earthquakes have longer durations.

32 *Uchide and Ide* [2010] compared the moment functions of $M_w 1.7-6.0$ events in Parkfield, California,
33 based on multi-scale inversion analyses. They pointed out that EL2 holds from the very early to later
34 stages of the source processes. *Meier et al.* [2016] demonstrated that peak ground displacement evolves
35 with the cube law. As the far-field ground displacement is proportional to STFs, they suggested that
36 the law is sourced from the phenomenon of self-similar rupturing of the fault, which results in EL2.
37 In addition, the proportionality between the final moment and the cube of the total duration has been
38 established [e.g., *Houston*, 2001].

39 Given the spectra of STFs, their amplitudes above their corner frequencies can be modeled by a power
40 law, and their fall-off rates can be quantified. As shown by numerous studies [e.g., *Boatwright*, 1980;

41 *Abercrombie, 1995; Kanamori, 2014*], EL3 seems to be very robust. Some forward modeling studies of
42 dynamic rupturing have been conducted to explain the ω^{-2} -model; they have shown that STFs consist
43 of functions that are almost entirely smooth, except for a kink. For example, Brune's model has a kink
44 at its start, while Sato & Hirasawa's model and Madariaga's model both have a kink due to their stopping
45 phases [see the review of *Madariaga and Ruiz, 2016*, on each mathematical or numerical representa-
46 tion]. However, the cataloged STFs do not show such an isolated kink, but do show some fluctuations
47 [*Yin et al., 2021*]. This implies that the traditional modeling approaches are too simplified to reproduce
48 the complexity of STFs, and thus, that some stochastic modeling is required.

49 Apart from the entire shape of each STF as discussed above, it has been well established that EL4
50 holds. The GR law originally means that the probability density function (PDF) of a seismic moment is
51 a power law. By recalling the cube law between the moment and the duration, the GR law means that
52 the PDF of the duration is also a power law. Once we model stochastic STFs, we can estimate the PDF
53 of the duration and discuss whether the PDF satisfies the GR law.

54 The stochastic modeling of faulting processes has been proposed both theoretically and numerically.
55 *Andrews [1980, 1981]* considered a spatio-temporal slip distribution with self-affinity, mainly in the
56 Fourier domain. This approach revealed the spectra of the distribution and energetics of the faulting.
57 Significantly, the fault impedance, which is the factor of proportionality between the slip rate and stress
58 drop in the Fourier domain, can enlighten the relationship between the quantities, even in the stochas-
59 tic model. After *Andrews [1980, 1981]*, the importance of stochasticity has been more recognized (see
60 the introduction of *Aso et al. [2019]* for details). *Aso et al. [2019]* introduced temporal stochasticity
61 into their boundary integral equation for the dynamic rupture process and demonstrated the rupture
62 complexity. While such numerical modeling is developing, mathematical modeling, if available, would
63 contribute to the understanding of complex faulting processes.

64 Stochastic differential equation(SDE)-based models have been employed in the field of earthquake
65 source physics. *Matthews et al. [2002]* and *Ide [2008]* modeled recurrent and slow earthquakes, respec-
66 tively, as Brownian motion. *Matthews et al. [2002]* focused on regular earthquakes; however, the time

67 scale considered by them was longer than each event, and they did not consider the properties of STFs.
68 *Wu et al.* [2019] assumed that the generalized Langevin equation can model the equation of motion for
69 the fault slip rate. Although their model was based on some physical properties of dynamic friction,
70 their solution was Brownian motion, which cannot satisfy the non-negativeness (EL1) or the ω^{-2} -like
71 spectrum (EL3). Thus, a novel approach is need for SDE-based modeling under EL1–4.

72 In this article, we consider an SDE known as the Bessel process. We analytically and numerically
73 demonstrate that the convolution of two solutions from the same Bessel process satisfies EL1–4. Finally,
74 we discuss the physical meaning of these two solutions on the basis of the fault impedance.

75 **2 Mathematical modeling**

76 In the following, we do not distinguish $\text{STF} := \int_{\Gamma} V(\mathbf{x}, t) d\mathbf{x}$ and moment-rate function $\dot{M}(t) :=$
77 $\mu \int_{\Gamma} V(\mathbf{x}, t) d\mathbf{x}$ on a flat fault Γ , where μ is the rigidity and V is the slip rate distribution. We intro-
78 duce a mathematical model to generate $\dot{M}(t)$ that satisfies EL1–4 using solutions of an SDE. *Ide* [2008]
79 modeled \dot{M} for slow earthquakes as Brownian motion because the observed source spectra of slow
80 earthquakes follow the ω^{-1} -model, which is similar to the spectrum of Brownian motion. For regular
81 earthquakes, however, EL3 holds. Thus, we consider a product of the spectra of two stochastic processes
82 (i.e., $\omega^{-1} \times \omega^{-1} = \omega^{-2}$), which is a convolution of the two stochastic processes in the time domain, which
83 we denote as $X_t^{(1)}$ and $X_t^{(2)}$ herein. Thus, we assume that $\dot{M} = X_t^{(1)} * X_t^{(2)}$ holds, where the asterisk “*”
84 denotes the convolution in time.

85 To fulfill EL1, we assume that both $X_t^{(1)}$ and $X_t^{(2)}$ are solutions of the following SDE called the Bessel
86 process:

$$dX_t^{(i)} = \frac{d-1}{2} \frac{dt}{X_t^{(i)}} + dB_t^{(i)}, \quad (i = 1, 2) \quad (1)$$

87 with its initial value $X_0^{(i)} (> 0)$, which is equivalent to the integral form as:

$$X_t^{(i)} = X_0^{(i)} + B_t^{(i)} + \frac{d-1}{2} \int_0^t \frac{ds}{X_s^{(i)}}, \quad (i = 1, 2) \quad (2)$$

88 where $B_t^{(i)}$ is a standard Brownian motion and d is the dimension of the Bessel process. SDE(1) is
89 valid while $X_t^{(i)} > 0$ holds. Thus, we define $X_t^{(i)} = 0$ after the process hits zero; the time $T :=$

90 $\min_t \{t | t > 0 \& X_t^{(i)} = 0\}$ is referred to herein as the first hitting time [Göing-Jaeschke and Yor, 2003].
 91 According to the above definition, $X_t^{(i)}$ is continuous and non-negative. Moreover, $X_t^{(i)}$ with $d < 2$ is
 92 compactly supported because $T \ll \infty$ holds almost surely if $d < 2$ [Göing-Jaeschke and Yor, 2003].
 93 Therefore, given $d < 2$, EL1 holds if we can confirm that $X_t^{(1)} * X_t^{(2)}$ is unimodal. We demonstrate this
 94 statement numerically in the next section.

95 We also confirm that $X_t^{(1)} * X_t^{(2)}$ satisfies EL2 and EL3 numerically in the next section. It can be
 96 expected that EL3 would be satisfied, as described in the first paragraph of this section.

97 The condition for EL4 can be derived analytically. Hamana and Matsumoto [2013] showed that $P(T)$,
 98 which is the PDF of the first hitting time T with $d < 2$ and $X_0^{(i)} = a$, can be represented as:

$$P(T) = \frac{2^\nu}{a^2 \Gamma(|\nu|)} T^{\nu-1} \exp\left(-\frac{a^2}{2T}\right), \quad (3)$$

99 where $\nu = \frac{d}{2} - 1$, and $\Gamma(\cdot)$ is a gamma function. On the other hand, considering the cube law ($M_0 \sim T^3$),
 100 the GR law with respect to $M_w = \frac{2}{3} \log_{10} M_0 - 6.1$ can be represented as

$$P(M_w) \sim 10^{-bM_w} \sim T^{-2b}, \quad (4)$$

101 where $b \sim 1$ holds and the constant coefficients are neglected. Thus, if we assume a sufficiently small
 102 initial value, $a (\ll \sqrt{2T})$, eqs (3) and (4) imply that:

$$\nu = -2b + 1, \quad \text{i.e.,} \quad d = 4(1 - b) \quad (5)$$

103 is required for EL4.

104 3 Numerical Modeling and Results

105 In the following section, we investigate how the convolution $X_t^{(1)} * X_t^{(2)}$ satisfies EL1–3 after solving
 106 eq.(1) using the SRIW1 algorithm [Rößler, 2010] implemented in DifferentialEquations.jl (<https://diffeq.sciml.ai/>
 107) for Julia 1.6.1 (<https://julialang.org/>). Given eq.(5) and $b = 1$, we solve:

$$dX_t = -\frac{1}{2} \frac{dt}{X_t} + dB_t$$

108 with a constant time step of $dt = 10^{-6}$ and a sufficiently small initial value of $X_0 = 10^{-3}$ up to time
 109 $T_{\max} = 2 \times 10^{-3}$ (i.e., 2,000 steps). Because the solution must become zero in our model, we reject
 110 numerical solutions that never reached zero before T_{\max} . The convolution of two solutions does not
 111 follow ω^{-2} -model if their corner frequencies, which are comparable to the inverse of their first hitting
 112 time, are quite different. Thus, we denote the lower limit of the first hitting time as T_{\min} and reject
 113 solutions that reach zero before T_{\min} . In the following, we investigate two cases: A) $T_{\min} = 2 \times 10^{-4}$
 114 (i.e., 200 steps) and B) $T_{\min} = 1 \times 10^{-3}$ (i.e., 1,000 steps). Therefore, we consider the Bessel processes
 115 with the probabilistic first hitting time T satisfying $T_{\min} \leq T \leq T_{\max}$, where $T_{\min}/T_{\max} = 0.1$ for case A
 116 and $T_{\min}/T_{\max} = 0.5$ for case B. For every two solutions, we regard the solution with relatively shorter
 117 duration as $X_t^{(1)}$ and the other as $X_t^{(2)}$. Thus, $T_{\min}/T_{\max} \leq T_1/T_2 \leq 1$ holds, where T_i is the duration
 118 for $X_t^{(i)}$ ($i = 1, 2$).

119 After iterations, we store 2,000 solutions with $T_{\min} \leq T \leq T_{\max}$, which yields 1,000 pairs of solutions,
 120 and calculate 1,000 convolutions of the pairs. Even though we calculate and abandon many useless
 121 solutions, we obtain ~ 120 Bessel processes per minute within the duration range by using 12-core AMD
 122 Ryzen 9 3900XT.

123 The 1,000 convolutions dominantly satisfy EL1 (Fig.1), whereas the case B shows more variation (see
 124 Supporting Figures for individual cases). Simultaneously, the time integration (Fig.2) and Fourier am-
 125 plitude spectra (Fig.3) reproduce EL2 and EL3, respectively. EL4 is almost surely satisfied, as discussed
 126 in the previous section. Hence, we conclude that the convolution of two Bessel processes with $d = 0$
 127 stochastically fulfills EL1–EL4.

128 4 Discussion

129 Here, we interpret the physical meaning of the convolution of two Bessel processes. In the following,
 130 we consider a finite flat fault surface Γ and define two convolutions: “*” as only in time and “*” as in
 131 on-fault position and time. In the case of a finite fault, we assume that the stress drop rate, $\dot{\sigma}(\mathbf{x}, t)$ for

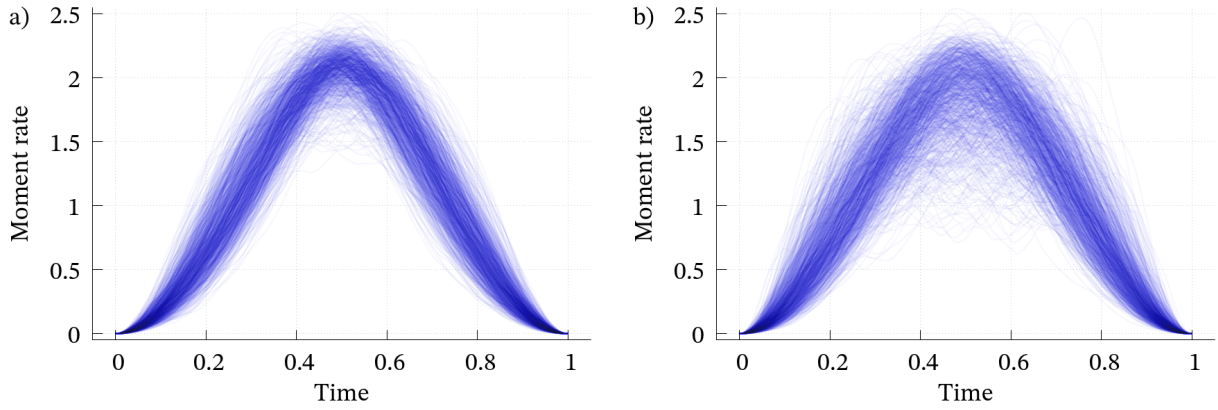


Figure 1: The 1,000 computed convolutions of the two Bessel processes for (a) case A and (b) case B.

Time scale and total moment are normalized.

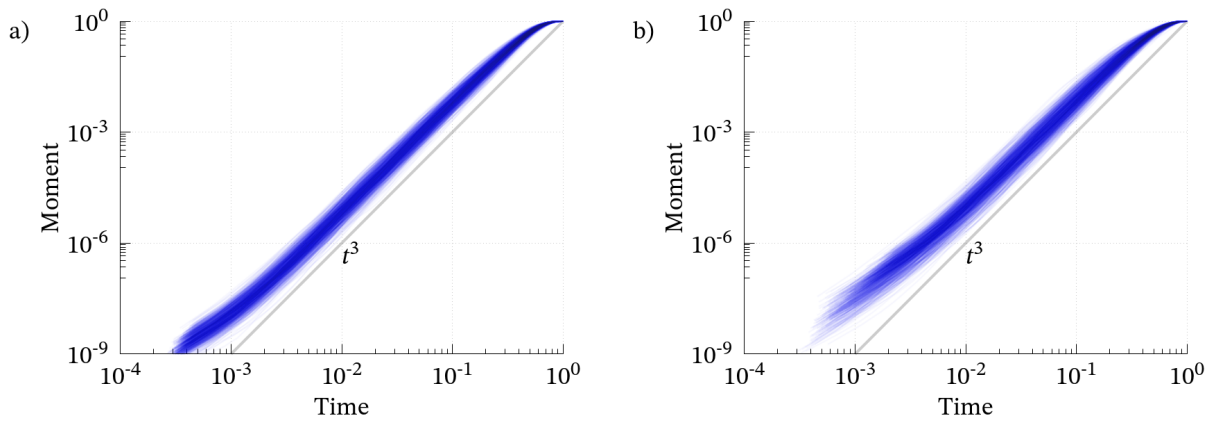


Figure 2: The normalized moment evolution $\left(\int_0^t \dot{M}(s) ds / \int_0^\infty \dot{M}(s) ds \right)$ for (a) case A and (b) case B along normalized time scale (t/T) . The curves dominantly follow the cube law $(\sim t^3)$ except for in their initial stages, which are affected by their initial values, and in their final stages, which converge toward their static states.

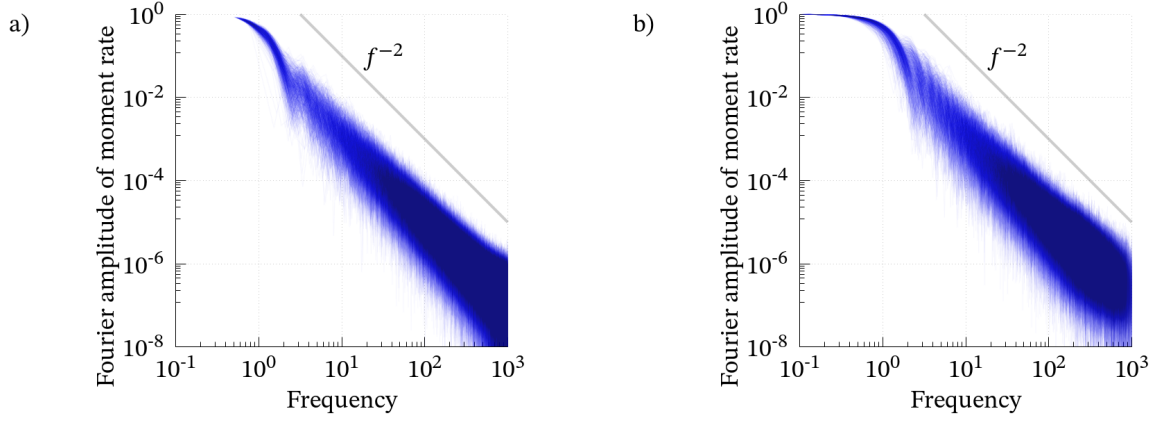


Figure 3: The normalized Fourier amplitude spectra of the convolutions plotted in Fig.1 for (a) case A and (b) case B.

132 the on-fault position $\mathbf{x} \in \Gamma$, can be represented as:

$$\dot{\sigma}(\mathbf{x}, t) = -(\dot{m} \tilde{*} Z)(\mathbf{x}, t), \quad (6)$$

133 where $\dot{m}(\mathbf{x}, t)$ is the moment-rate density function and $Z(\mathbf{x}, t)$ is the fault impedance, as detailed by
 134 *Andrews* [1980, 1981]. If the surrounding area is an elastic body, Z can be derived from linear elasticity.
 135 However, we consider a stochastic process in which Z includes a non-deterministic property. Eq.(6) rep-
 136 resents the stress rate (i.e., Neumann condition) based on the displacement discontinuity (i.e., Dirichlet
 137 condition) along a finite fault; thus, Z is called a Dirichlet-to-Neumann operator. Here, we assume that
 138 there exists a Neumann-to-Dirichlet operator Z^{-1} , whose support is Γ , satisfying:

$$\dot{m}(\mathbf{x}, t) = -(\dot{\sigma} \tilde{*} Z^{-1})(\mathbf{x}, t). \quad (7)$$

139 Furthermore, the Fourier transform with respect to position ($\int_{\Gamma} e^{2\pi i \mathbf{k} \cdot \mathbf{x}} d\mathbf{x}$, where \mathbf{k} is a two dimensional
 140 wavenumber) yields:

$$\dot{m}(\mathbf{k}, t) = -(\dot{\sigma}(\mathbf{k}, \cdot) * Z^{-1}(\mathbf{k}, \cdot))(t). \quad (8)$$

141 As the limit $\mathbf{k} \rightarrow 0$ is equivalent to the integration in space ($\lim_{\mathbf{k} \rightarrow 0} \int_{\Gamma} e^{2\pi i \mathbf{k} \cdot \mathbf{x}} d\mathbf{x} = \int_{\Gamma} d\mathbf{x}$), eq.(8) results
 142 in

$$\overline{\dot{m}}(t) = \dot{M}(t) = -(\overline{\dot{\sigma}} * \overline{K^{-1}})(t), \quad (9)$$

143 where the overlines denote integration over Γ . Finally, eq.(9) implies that EL1-4 are fulfilled if the stress
 144 rate, $\overline{\dot{\sigma}}(t)$, and Neumann-to-Dirichlet operator, $\overline{Z^{-1}}$, when integrated over Γ , are Bessel processes.

145 As σ comprises stress *drop*, $-\bar{\sigma}(t)$ is always non-negative and $-\bar{\sigma}(t)$ is a non-decreasing function
 146 from zero to its final value (> 0). This property is naturally produced if $-\dot{\bar{\sigma}}(t)$ is a Bessel process.
 147 For the 1,000 results, $X_t^{(1)} * X_t^{(2)}$, as obtained in the previous section, we also calculate $-\int_0^t X_s^{(1)} ds$,
 148 where the duration of $X_s^{(1)}$ is shorter than that of $X_s^{(2)}$. By considering this quantity as $\bar{\sigma}(t)$, we confirm
 149 the relationship between $M(t)$ and $\bar{\sigma}(t)$. The results show monotonic slip-weakening curves (Fig.4).
 150 Therefore, the assumption that the stress drop rate is a Bessel process explains the natural weakening
 151 process of the on-fault stress change. In Fig.4, the abscissa and ordinate mimic averaged slip and stress
 152 drop over the fault, respectively. This means that the characteristic slip weakening distance ranges
 153 from 20% to 50% of the final slip amount. Interestingly, this fraction is close to results obtained based
 154 on observations [e.g., *Mikumo*, 2003].

155 To interpret the other assumption that the inverse fault impedance, $\overline{Z^{-1}}$, is a random process is not
 156 straightforward. When we calculate seismic waves, the Green functions are well modeled within the
 157 framework of linear elasticity. This might be because the Green functions depend on the medium be-
 158 tween the fault and (usually) far-field observation points, where almost all of the region is an elastic
 159 body. However, the (inverse) fault impedance is a propagator among the on-fault positions traveling
 160 along the fault. In general, faults are segmented, bumpy, and surrounded by fractured rocks. Modeling
 161 such a complex system by assuming a flat fault may cause non-deterministic fluctuations due to scat-
 162 tering waves, as schematically illustrated by *Aso et al.* [2019]. Therefore, this assumption is possible,
 163 even though it is difficult to directly observe.

164 In the numerical simulation, we restrict the ratio of the duration of $X_t^{(1)}$ and $X_t^{(2)}$ within tenfold. This
 165 is not only for EL3, as mentioned here, but also for another physical property. If $X_t^{(1)}$ is the stress drop
 166 rate, its duration should correspond to the duration of the most energetic faulting process, which is
 167 given by the fault length divided by the rupture speed. On the other hand, because $\overline{Z^{-1}}(t) = X_t^{(2)}$ is
 168 based on the fault impedance, its duration must be equivalent to the time taken for the scattering wave
 169 to spread over the entire fault. This time is at least, or even a few times greater than, the fault length
 170 divided by the seismic wave speed. Therefore, the durations of $X_t^{(1)}$ and $X_t^{(2)}$ should have almost the

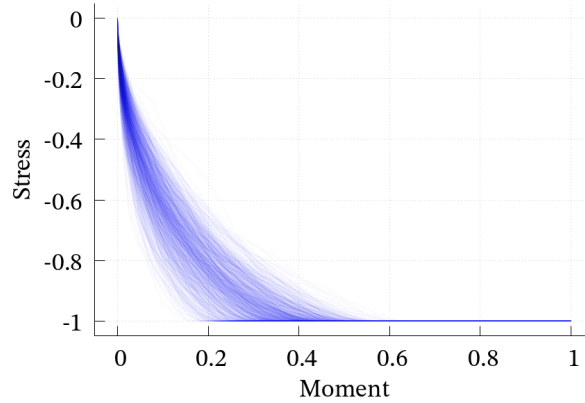


Figure 4: Normalized moment versus normalized stress drop assumed to be time-integration of a Bessel process for case A.

171 same order, and $T_{\min}/T_{\max} = 0.1$ and 0.5 in our assumption might be two possible end members.

172 5 Conclusions and outlooks

173 Here we demonstrate that the four empirical laws on STFs, or moment-rate functions, can be repro-
 174 duced by modeling STFs as the convolution of two Bessel processes with almost the same order of
 175 duration. In terms of fault mechanics, given the complexity of the geometry and surroundings of the
 176 faults, this result is comprehensible if both the stress drop rate and the inverse fault impedance follow
 177 a Bessel process.

178 One possible future approach could be to extend the model by considering spatial heterogeneity of
 179 stress, fault geometry, and the surrounding medium. This is similar to the numerical model of *Aso*
 180 *et al.* [2019]; further mathematical model and results will broaden our understanding. The main diffi-
 181 culty might be that we must somehow consider a stochastic partial differential equation that considers
 182 both space and time, which is a more mathematically challenging task. Were such a model available,
 183 it would be possible to discuss the physical processes related to rupture initiation, propagation, and
 184 termination as stochastic processes. Moreover, some relationships between the kinetic and potential
 185 energies released from heterogeneous slip distribution [e.g., *Hirano and Yagi, 2017*] could be revealed,
 186 which would be necessary for the energetics of faulting.

187 A future plan could be to apply our model to scientific and engineering studies on strong ground mo-
188 tions. One way to numerically simulate strong ground motions is to compute the convolution of an STF
189 and the Green function. However, this STF should not be unique, even if we consider a single fault, and
190 stochastic simulation would be required by assuming various STFs. Our model allows us to generate
191 numerous STFs using a the stochastic process that leads to statistical analyses. In general, even without
192 numerous numerical simulations, we can investigate the statistical properties of a stochastic process if
193 the PDF of the random variable at any time is available by solving the corresponding Fokker-Planck
194 equation. Fortunately, the PDF for the Bessel process is already known [Guarnieri *et al.*, 2017]. Thus, it
195 should be possible to calculate some statistical properties of strong ground motion at low computational
196 costs.

197 **acknowledgments**

198 This work was supported by JSPS KAKENHI Grant (18K13637) and the Japan–Russia Research Coop-
199 erative Program (JSPS and RFBR, project No. J19–721). The author has no conflict of interest, financial
200 or otherwise. No data were used in this study.

201 **References**

- 202 Abercrombie, R. E., Earthquake source scaling relationships from -1 to $5 M_L$ using seismograms
203 recorded at 2.5-km depth, *Journal of Geophysical Research: Solid Earth*, 100(B12), 24,015–24,036,
204 doi:10.1029/95jb02397, 1995.
- 205 Andrews, D. J., Fault impedance and earthquake energy in the Fourier transform domain, *Bulletin of*
206 *the Seismological Society of America*, 70(5), 1683–1698, 1980.
- 207 Andrews, D. J., A stochastic fault model: 2. time-dependent case, *Journal of Geophysical Research: Solid*
208 *Earth*, 86(B11), 10,821–10,834, doi:10.1029/jb086ib11p10821, 1981.
- 209 Aso, N., R. Ando, and S. Ide, Ordinary and slow earthquakes reproduced in a simple continuum system

210 with stochastic temporal stress fluctuations, *Geophysical Research Letters*, 46(24), 14,347–14,357, doi:
211 10.1029/2019gl085010, 2019.

212 Boatwright, J., A spectral theory for circular seismic sources; simple estimates of source dimension,
213 dynamic stress drop, and radiated seismic energy, *Bulletin of the Seismological Society of America*,
214 70(1), 1–27, 1980.

215 Göing-Jaeschke, A., and M. Yor, A survey and some generalizations of Bessel processes, *Bernoulli*, 9(2),
216 doi:10.3150/bj/1068128980, 2003.

217 Guarnieri, F., W. Moon, and J. S. Wettlaufer, Solution of the Fokker-Planck equation with a logarithmic
218 potential and mixed eigenvalue spectrum, *Journal of Mathematical Physics*, 58(9), 093,301, doi:
219 10.1063/1.5000386, 2017.

220 Hamana, Y., and H. Matsumoto, The probability distributions of the first hitting times of Bessel pro-
221 cesses, *Transactions of the American Mathematical Society*, 365(10), 5237–5257, doi:10.1090/s0002-
222 9947-2013-05799-6, 2013.

223 Hirano, S., and Y. Yagi, Dependence of seismic and radiated energy on shorter wavelength components,
224 *Geophysical Journal International*, 209(3), 1585–1592, doi:10.1093/gji/ggx108, 2017.

225 Houston, H., Influence of depth, focal mechanism, and tectonic setting on the shape and duration of
226 earthquake source time functions, *Journal of Geophysical Research: Solid Earth*, 106(B6), 11,137–
227 11,150, doi:10.1029/2000jb900468, 2001.

228 Ide, S., A Brownian walk model for slow earthquakes, *Geophysical Research Letters*, 35(17), doi:
229 10.1029/2008gl034821, 2008.

230 Kanamori, H., The diversity of large earthquakes and its implications for hazard mitigation, *Annual*
231 *Review of Earth and Planetary Sciences*, 42(1), 7–26, doi:10.1146/annurev-earth-060313-055034, 2014.

232 Madariaga, R., and S. Ruiz, Earthquake dynamics on circular faults: a review 1970–2015, *Journal of*
233 *Seismology*, 20(4), 1235–1252, doi:10.1007/s10950-016-9590-8, 2016.

- 234 Matthews, M., W. Ellsworth, and P. Reasenber, A Brownian model for recurrent earthquakes, *Bulletin*
235 *of the Seismological Society of America*, 92(6), 2233–2250, doi:10.1785/0120010267, 2002.
- 236 Meier, M.-A., T. Heaton, and J. Clinton, Evidence for universal earthquake rupture initiation behavior,
237 *Geophysical Research Letters*, 43(15), 7991–7996, doi:10.1002/2016gl070081, 2016.
- 238 Mikumo, T., Stress-breakdown time and slip-weakening distance inferred from slip-velocity func-
239 tions on earthquake faults, *Bulletin of the Seismological Society of America*, 93(1), 264–282, doi:
240 10.1785/0120020082, 2003.
- 241 Rößler, A., Runge–Kutta methods for the strong approximation of solutions of stochastic differential
242 equations, *SIAM Journal on Numerical Analysis*, 48(3), 922–952, doi:10.1137/09076636x, 2010.
- 243 Uchide, T., and S. Ide, Scaling of earthquake rupture growth in the Parkfield area: Self-similar growth
244 and suppression by the finite seismogenic layer, *Journal of Geophysical Research*, 115(B11), doi:
245 10.1029/2009jb007122, 2010.
- 246 Wu, T.-H., C.-C. Chen, M. Lovallo, and L. Telesca, Informational analysis of Langevin equation of
247 friction in earthquake rupture processes, *Chaos: An Interdisciplinary Journal of Nonlinear Science*,
248 29(10), 103,120, doi:10.1063/1.5092552, 2019.
- 249 Yin, J., Z. Li, and M. A. Denolle, Source time function clustering reveals patterns in earthquake dynam-
250 ics, *Seismological Research Letters*, 92, 2343–2353, doi:10.1785/0220200403, 2021.